

# Target Tracking with Binary Proximity Sensors: Fundamental Limits, Minimal Descriptions, and Algorithms\*

N. Shrivastava

Dept. of Computer Science  
Univ. of California  
Santa Barbara, CA 93106, USA  
nisheeth@cs.ucsb.edu

R. Mudumbai U. Madhow

Dept. of Elec. & Comp. Engr.  
Univ. of California  
Santa Barbara, CA 93106, USA  
{madhow,raghu}@ece.ucsb.edu

S. Suri

Dept. of Computer Science  
Univ. of California  
Santa Barbara, CA 93106, USA  
suri@cs.ucsb.edu

## Abstract

We explore fundamental performance limits of tracking a target in a two-dimensional field of binary proximity sensors, and design algorithms that attain those limits. In particular, using geometric and probabilistic analysis of an idealized model, we prove that the achievable spatial resolution  $\Delta$  in localizing a target's trajectory is of the order of  $\frac{1}{\rho R}$ , where  $R$  is the sensing radius and  $\rho$  is the sensor density per unit area. Using an Occam's razor approach, we then design a geometric algorithm for computing an economical (in descriptive complexity) piecewise linear path that approximates the trajectory within this fundamental limit of accuracy. We employ analogies between binary sensing and sampling theory to contend that only a "lowpass" approximation of the trajectory is attainable, and explore the implications of this observation for estimating the target's velocity.

We show through simulation the effectiveness of the geometric algorithm in tracking both the trajectory and the velocity of the target for idealized models. For non-ideal sensors exhibiting sensing errors, the geometric algorithm can yield poor performance. We show that non-idealities can be handled well using a particle filter based approach, and that geometric post-processing of the output of the Particle Filter algorithm yields an economical path description as in the idealized setting. Finally, we report on our lab-scale experiments using motes with acoustic sensors to validate our theoretical and simulation results.

---

\*This work was supported by the National Science Foundation under grants ANI-0220118, CCF-0431205, CNS-0520335, CCF 0514738, the Office of Naval Research under grant N00014-06-0066, and by the Institute for Collaborative Biotechnologies through grant DAAD19-03-D-0004 from the U.S. Army Research Office.

Permission to make digital or hard copies of all or part of this work for personal or classroom use is granted without fee provided that copies are not made or distributed for profit or commercial advantage and that copies bear this notice and the full citation on the first page. To copy otherwise, to republish, to post on servers or to redistribute to lists, requires prior specific permission and/or a fee.  
SenSys'06, November 1–3, 2006, Boulder, Colorado, USA.  
Copyright 2006 ACM 1-59593-343-3/06/0011 ...\$5.00

## Categories and Subject Descriptors

H.1.1 [Systems and Information Theory]: Information theory, Value of information

## General Terms

Algorithms, Theory

## Keywords

Sensor Networks, Target Tracking, Binary Sensing, Fundamental Limits, Distributed Algorithms

## 1 Introduction

We investigate the problem of target tracking using a network of binary proximity sensors: each sensor outputs a 1 when the target of interest is within its sensing range, and 0 otherwise. This simple sensing model is of both fundamental and practical interest for several reasons. First, because of the minimal assumption about the sensing capability, it provides a simple and robust abstraction for a basic tracking architecture of broad applicability, which can be enhanced in a situation-specific fashion to take advantage of additional information such as target velocity or distance, if available. Second, the communication requirements for the binary proximity model are minimal—each sensor can smooth out its noisy observations and express its output as one or more disjoint intervals of time during which the target is in its range, which can be encoded efficiently by timestamps when the output changes from 0 to 1 and vice versa. Finally, the simplicity of the model permits the derivation of intuitively attractive performance limits, which serve both to guide design of tracking algorithms and to provide lower bounds on tracking performance with more sophisticated sensors.

We begin by exploring the fundamental limit of *spatial resolution* that can be achieved in tracking a target within a two-dimensional field of binary proximity sensors. The spatial resolution measures the accuracy with which a target's trajectory can be tracked, and it is defined as the worst-case deviation between the estimated and the actual paths. We prove that the ideal achievable resolution  $\Delta$  is of the order of  $\frac{1}{\rho R}$ , where  $R$  is the sensing range of individual sensors and  $\rho$  is the sensor density per unit area. This result articulates the common intuition that, for a fixed sensing radius, the accuracy improves linearly with an increasing sensor density. But

it also shows that, for a fixed number of sensors, the accuracy improves linearly with an increase in the sensing radius, which occurs because an increase in the sensing radius leads to a finer *geometric partition* of the field. Our spatial resolution theorem helps explain empirical observations reported in prior work on tracking in binary sensor networks [12].

Next, we consider minimal representations and velocity estimation for the target’s trajectory. There are infinitely many candidate trajectories consistent with the sensor observations and within the guaranteed spatial resolution of the true trajectory, and all of which are “good enough” for localization accuracy. On the other hand, the velocity estimation for the target depends crucially on the shape of the trajectory. We use an analogy between binary sensing and the sampling theory and quantization to argue that “high-frequency” variations in the target’s trajectory are invisible to the sensor field at a spatial scale smaller than the resolution  $\Delta$ . Therefore, we can only hope to estimate the shape or velocity for a “low-pass” version of the trajectory.<sup>1</sup> We then consider piecewise linear approximations to the trajectory that can be described economically. We give sufficient conditions for the lowpass version of the true target trajectory under which such minimal representations can estimate the velocity accurately.

Our results on velocity estimation can be paraphrased as follows: velocity estimates for a segment of the trajectory approximated by a straight line are good if the segment is long enough. This motivates an Occam’s razor approach for describing the trajectories in terms of piecewise linear paths in which the line segments are as long as possible, without exceeding the approximation error limit provided by our spatial resolution theorem. We develop the OCCAMTRACK algorithm, which efficiently computes such piecewise linear trajectories, and associated velocity estimates, from the sensor observations. The efficacy of the algorithm in achieving the fundamental limits on spatial resolution and velocity estimation error is demonstrated via simulations.

Next, we consider more realistic sensor models, in which the coverage areas for different sensors may be different, and not exactly known to the tracker node. For such non-ideal sensors exhibiting sensing errors, the OCCAMTRACK algorithm can yield poor performance. We show that sensor non-idealities can be handled well using a particle filter approach adapted to non-ideal binary sensing. While this particle filter algorithm is robust to nonidealities, the paths it outputs are not smooth, and therefore not easy to describe economically. We show that geometric post-processing of the output of the particle filtering algorithm leads again to minimal representations in terms of piecewise linear trajectories with a small number of line segments, with the required goodness of fit guided by the fundamental limits on spatial resolution. Simulations are used to demonstrate the effectiveness of the overall algorithm in providing accurate tracking with minimal path representations.

Finally, we carried out a lab-scale demonstration with motes equipped with acoustic sensors for a quick validation of our framework. We found that the coverage area varies

<sup>1</sup>A technical definition of the lowpass trajectory is given in Section 3.4.1.

significantly across sensors, and exhibits nonmonotonicity: the probability that a target is detected does not necessarily go down monotonically with distance from the sensor. We employed two approaches to deal with real-world noisy data: (i) preprocessing of the noisy sensor outputs to clean up obvious error patterns, followed by the OCCAMTRACK algorithm, and (ii) the Particle Filter algorithm followed by geometric post-processing. Both these approaches show good tracking performance.

## Related Work

Object tracking has long been an active area of research for battle-field [9], robotics [16] and other applications. Any sensor that generates a signal dependent on distance from a target can be used for tracking. Accordingly different sensing modalities such as radar, acoustic, ultrasonic, magnetic, seismic, video, RF and infrared [15], and occasionally combinations of multiple modalities [3], have been considered for tracking applications in both theory and practice. The range and capabilities of these sensors vary widely, and many different approaches to modeling and data processing have been investigated. For instance, ultrasonic signals carry rich information about the range of the object, whereas infrared sensors are best modeled as detectors or binary sensors [17]. We do not attempt to do justice to the vast literature on tracking, but briefly review closely related work.

The robustness and effectiveness of tracking using binary sensing models has been convincingly demonstrated for a large-scale sensor network in [1]. The success of this project provides strong motivation for the fundamental exploration of binary sensing undertaken here. The authors of [12] consider a model identical to ours. They employ piecewise linear path approximations computed using variants of a weighted centroid algorithm, and obtain good tracking performance if the trajectory is smooth enough. Our fundamental limits provide an explanation for some of the empirical observations in [12], while our algorithms provide more accurate and more economical path descriptions. Another closely related paper is [2], which considers a different sensing model, where sensors provide information as to whether a target is moving towards or away from them. While the specific results for this model are quite different from ours, the philosophy is similar in that the authors of [2] use geometric analysis to characterize fundamental limits. However, the sensing model in [2] can lead to unacceptable ambiguities in the target’s trajectory (the authors offer an example of parallel trajectories that are indistinguishable without additional proximity information). In contrast, the binary proximity model considered here, despite its minimalism, is able to localize the target to within a spatial resolution  $O(\frac{1}{\rho R})$ . In [13], Liu et al. present some interesting ideas using geometric duality to track moving shadows in a network of binary sensors. Although their technique is not applicable to our problem setting, their notion of cells in dual space has some resemblance to our localization patches.

Classical tracking is often formulated as a Kalman filtering problem, using Gaussian models for sensor measurements and the target trajectory. Distributed tracking based on Kalman filtering has recently been considered in [14].

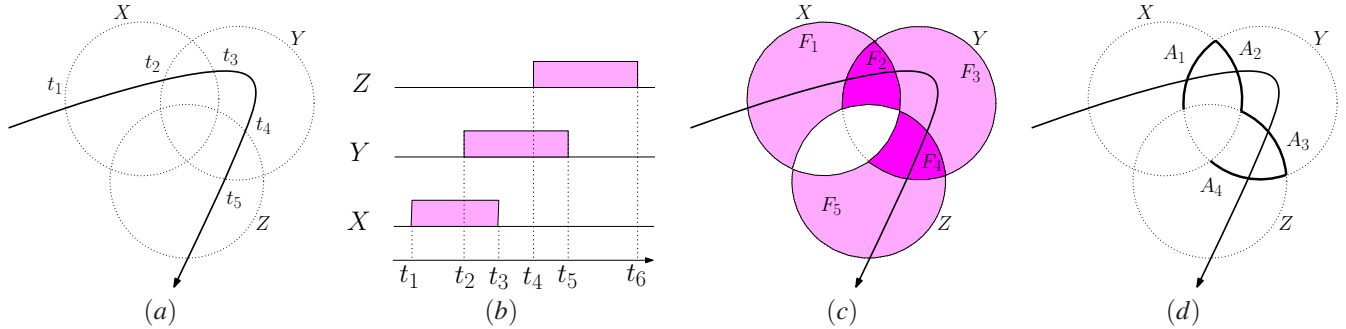


**Figure 1.** A target moving through a field of three binary proximity sensors,  $X$ ,  $Y$  and  $Z$ ; (b) shows sensor outputs as a function of time; (c) shows the *localization patches* to which the target is localized over time intervals with constant signature; and (d) shows the *arcs* marking boundaries between patches.

Particle filters [5] offer an alternative to Kalman filters in non-Gaussian setting, and have been investigated for tracking using sensor networks in [4]. Most prior work on particle filtering assumes more sensed information (with a more detailed probabilistic model) than provided by the binary sensing model of this paper. Khan et al. [10, 11] have used particle filtering for an insect tracking application, where the insect targets are assumed to interact according to a Markov random field. Fox et al. [7] provide a survey of particle-filter based methods for the problem of mobile robot localization, where robots wish to determine their location, and the locations of other robots, using sensory inputs. Our contribution in this paper is to provide a particularly simple particle filtering algorithm that provides robust performance using the minimal information obtained from non-ideal binary sensors.

## 2 The Geometry of Binary Sensing

In this section, we describe an idealized model for a binary sensor network, and the structure of the geometric information it provides regarding a target’s location. This geometric structure forms the basis for our theoretical bounds and algorithms.

Consider a network of  $n$  sensors in a two-dimensional plane. Each sensor detects an object within its *sensing region*, and generates one bit of information (1 for presence and 0 for absence) about the target; we call this the *ideal binary sensing model*. We get no other information about the location, speed, or other attributes of the target. The information of a sensor is efficiently encoded by the transitions between its 0 and 1 bits, and so its output can be summarized by the timestamps marking these transitions. We assume that the sensors are synchronized in time to sufficient accuracy—several timing synchronization algorithms are available in the literature (e.g., [6]). We also assume that the location of each sensor is known—the sensor locations can be recorded at the time of deployment, or can be estimated using localization techniques (e.g., [18]).

Our emphasis is on discovering and attaining fundamental limits of tracking performance, and therefore we abstract away lower layer networking issues by assuming that the sensor observations are communicated to, and fused at, a

*tracker node*. Given the minimal communication needs of binary proximity sensors, such a centralized architecture may well be the most attractive choice for implementation in many settings, using multihop wireless communication between the sensors and the tracker node(s). In any case, it is relatively straightforward to develop communication- and storage-efficient hierarchical distributed versions of our centralized algorithms: for example, the tracker node can be chosen dynamically based on the target’s location, and it can convey its summary of the particular segment of the target’s trajectory to the next tier of the hierarchy.

For simplicity, we assume that each sensor has a circular sensing region of radius  $R$ : a sensor outputs a 1 if a target falls within the *sensing disk* of radius  $R$  centered at its location. The parameter  $R$  is termed the *sensing range*. However, our framework also applies to sensing regions of more complex shapes that could vary across sensors. We assume noiseless sensing for the time being: the sensor output is always 1 if a target is within its sensing range, and always 0 if there is no target within its sensing range, with 100% accuracy. Methods for handling noisy sensor readings are considered in later sections.

The geometry of binary sensing is best illustrated via an example. Figure 1(a) shows a target moving through an area covered by three sensors. Figure 1(b) shows the sensor outputs as a function of time. We define the *signature* of any point  $p$  in two-dimensional space as the  $n$ -bit vector of sensor readings, whose  $i$ th position represents the binary output of sensor  $i$  for a target at location  $p$ .<sup>2</sup> In Figure 1, if we define the signature as the bits output by sensors  $X$ ,  $Y$  and  $Z$  in that order, then the target’s signature evolves over time as follows: 000, 100, 110, 010, 011, 001, 000. Initially, it is outside the sensing disks of all three sensors; then it enters the disk of  $X$ , then  $Y$ , then it leaves the disk of  $X$ , enters that of  $Z$ , and so on. The time instants  $\{t_j\}$  mark the transitions when the target either enters or leaves a sensor’s range. Figure 1(c) shows that the target can be localized within a *localization patch*  $F_j$  during the time interval  $[t_j, t_{j+1})$ , which

<sup>2</sup>The notion of signature is a conceptual tool. Our algorithms do not actually use the entire bitmap for a given target location, but work with a much smaller localized version, as explained in the next section.

corresponds to the set of possible locations corresponding to the signature during this interval. When the target moves from a patch  $F_j$  to the next patch  $F_{j+1}$ , we note that exactly one sensor's bit changes: either the target enters the sensing disk of some sensor, or it leaves the disk of some sensor. The two patches,  $F_j$  and  $F_{j+1}$ , therefore, share a *localization arc*  $A_j$  of the disk of the sensor whose reading has flipped, as shown in Figure 1(d). A simple but important observation is that, at the transition times  $t_j$ , the two-dimensional uncertainty in the target's location is reduced to a one-dimensional uncertainty.

In general, a localization patch need not be connected and, correspondingly, the localization arc of two such patches can also have two or more pieces. (As a simple example, consider three sensing disks  $A, B, C$ , respectively, centered at points  $(0, 0)$ ,  $(1, 0)$ , and  $(2, 0)$ , where the radius of the disks is 1.5. Then, the patch with signature  $(0, 1, 0)$  has two disconnected pieces—these are the regions that are inside disk  $B$  but outside  $A$  and  $C$ .) Although disconnected patches are mainly an artifact of low sensor density, one can also create pathological examples where a patch can have two pieces even under high density. The non-connectivity of patches, however, does not impact the tracking resolution, because our Theorem 2 ensures that even if a patch is disconnected, all of its pieces lie within the resolution bound of each other.

The preceding geometric information structure forms the basis for our results in subsequent sections. Our derivation of fundamental limits in Section 3 is based on estimation of the size of the regions  $F_j$ . The geometric algorithms for computing minimal description trajectory estimates consist of computing piecewise linear approximations that pass through the patches  $F_j$  or the arcs  $A_j$  in the order specified by the evolution of the target's signature.

### 3 Fundamental Limits

We assume ideal sensing with sensing range  $R$  for each sensor, and an average sensor density of  $\rho$  sensors per unit area. Thus, the performance limits we derive depend only on the parameters  $\rho$  and  $R$ . We first show that the spatial resolution cannot be better than order of  $\frac{1}{\rho R}$ , regardless of the spatial distribution of the sensors. We then show that this resolution can be achieved using standard uniform random distributions as well as regular grids. Finally, we show that binary sensing is analogous to discrete sampling, in that it provides information only about a “lowpass” version of the target's trajectory, and discuss the implications for obtaining minimal path representations and velocity estimates.

#### 3.1 An Upper Bound on Spatial Resolution

The *localization error* of an estimated trajectory is defined to be the maximum deviation of the estimated path from the actual path. This is just the  $L_\infty$  norm of the difference between the actual and estimated trajectories, viewed as functions of time. The *spatial resolution* of a binary sensor field is the worst-case localization error for any target trajectory through the field.

As observed in Section 2, binary sensing localizes a target to within a *patch* corresponding to a specific signature, or bit

vector of sensor outputs. The spatial resolution is therefore given by the *diameter* of the largest patch induced by the binary sensing field. In the following, we argue that in *any* configuration of sensors, this diameter is *lower bounded* by  $\frac{c}{\rho R}$ , for an absolute constant  $c$ , which gives an *upper bound* on the achievable resolution.

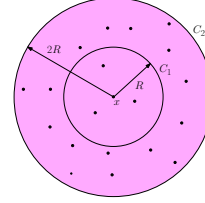


Figure 2. Illustration for Theorem 1.

**THEOREM 1.** *If a network of binary proximity sensors has average sensor density  $\rho$  and each sensor has sensing radius  $R$ , then the worst-case  $L_\infty$  error in localizing the target is at least  $\Omega(1/\rho R)$ .*

**PROOF.** We are interested in asymptotic behavior and so we assume that the sensor field is large relative to  $R$ , and we can ignore the boundary behavior by focusing on the portion of the field that is at least  $R$  away from the boundary. Since the average sensor density is  $\rho$  in the field, there must be a circular region of radius  $2R$  that contains at most (the average number of)  $N = \rho(4\pi R^2)$  sensors in it. Let  $x$  be the center of this circle, let  $C_1$  denote the circle of radius  $R$  centered at  $x$ , and let  $C_2$  be the circle of radius  $2R$  centered at  $x$ . (See Fig. 2 for illustration.) We observe that only the sensors contained in  $C_2$  can sense a target that lies in  $C_1$ . Since there are at most  $N$  such sensors, their sensing disks can partition the inner circle  $C_1$  into at most  $N^2 - N + 2$  “patches”. On the other hand, the circle  $C_1$  has area  $\pi R^2$ , so at least one of the patches must have area at least  $c\pi R^2/N^2$ , for some constant  $c$ . Plugging in the value of  $N$ , we get that some patch in  $C_1$  must have area at least

$$\frac{c\pi R^2}{16\pi^2 \rho^2 R^4} = \Omega\left(\frac{1}{\rho^2 R^2}\right).$$

Therefore, the *diameter* (the longest projection) of this patch is at least  $\Omega(\frac{1}{\rho R})$ , the square root of the area, which proves the claim.  $\square$

Theorem 1 makes no assumptions on the distribution of sensors: it only makes use of the average sensor density bound, and upper bounds the best resolution one can hope to achieve in an ideal deployment. In the next subsection, we address the complementary question: is this ideal resolution achievable, and what distributions of sensor nodes can realize this? Our investigation here is analytic, with a goal to show that certain simple configurations of sensors lead to regions where the maximum  $L_\infty$  error matches the bound of Theorem 1. Algorithmic questions of computing compact trajectory approximations are addressed in the following section.

### 3.2 Achievability of Spatial Resolution Bound

The spatial resolution of Theorem 1 can be achieved (neglecting edge effects) by simply arranging the sensors in a regular grid. Since such an ideal deployment is often impossible in practice, we now show that a random Poisson distribution with density  $\rho$  also achieves the desired resolution. In the process, we also derive a sharp tail bound on the size of a localization patch.

Mathematically, the Poisson distribution of mean  $\rho$  means that (i) the number of sensors in a region of area  $A$  is a Poisson random variable  $N_A$  with mean  $\rho A$ , and (ii) for two *nonoverlapping* regions, the corresponding numbers of sensors are independent random variables. We assume an asymptotic regime in which the probability of a point in the plane being within range of at least one sensor tends to one. For an arbitrary point  $P$ , this condition is satisfied if there is at least one sensor in a disk of radius  $R$  centered at  $P$ . Thus,  $P[\text{no sensor in disk of radius } R] = e^{-\rho\pi R^2} \rightarrow 0$  which requires that  $\rho R^2 \rightarrow \infty$ . (In practice, values of  $\rho R^2$  of the order of 4 or more suffice to guarantee adequate coverage). The following theorem states our result.

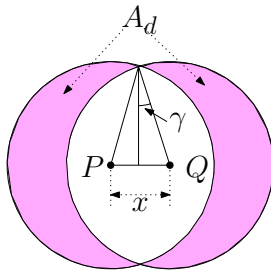


Figure 3. Illustration for proof of Theorem 2.

**THEOREM 2.** Consider a network of binary proximity sensors, distributed according to the Poisson distribution of density  $\rho$ , where each sensor has sensing radius  $R$ . Then the localization error at any point in the plane is of order  $\frac{1}{\rho R}$ .

**PROOF.** See Figure 3 for an illustration. Consider an arbitrarily chosen point  $P$  in the plane, and an arbitrarily chosen direction of movement, starting from that point. Given the isotropic nature of the Poisson distribution, without loss of generality, this direction can be chosen as going right along the horizontal direction. Let  $X$  denote the minimum movement required in that direction before there is a change in signature (i.e., before the boundary of some sensor’s disk is crossed). We wish to characterize the tail of the distribution of  $X$ .

To this end, consider a point  $Q$  that is a distance  $x$  away from  $P$  along the direction of movement, as shown in Figure 3. Any sensor detecting  $P$  (resp.  $Q$ ) must lie in the disk of radius  $R$  with center at  $P$  (resp.  $Q$ ). Thus,  $P$  and  $Q$  have the same signature if and only if the symmetric difference of these two disks (the shaded region in Figure 3) contains no sensor, assuming that either  $P$  or  $Q$  is detected by at least one sensor. (Under the assumption that  $\rho R^2$  is large, the last condition is met with high probability.) Letting  $A_d$  and  $A_u$ ,

respectively, denote the area of the symmetric difference and the union of the two disks, it follows from the Poisson distribution that

$$P[X > x] = e^{-\rho A_d} \frac{1 - e^{-\rho(A_u - A_d)}}{1 - e^{-\rho A_u}}, \quad 0 \leq x \leq 2R$$

(We note that  $A_d \leq A_u$ , with equality for  $x \geq 2R$ , so that  $P[X > x] = 0$  for  $x \geq 2R$ . Thus,  $X$  is upper-bounded by  $2R$ .) Elementary geometric calculations yield that

$$A_d = (2\gamma + \sin 2\gamma) R^2$$

where  $\gamma$  is the angle shown in Figure 3, satisfying  $\sin \gamma = \frac{x}{2R}$ . For our purpose, it suffices to loosely bound  $A_d$  below as

$$A_d \geq 2R^2 \sin \gamma = xR$$

(using  $\gamma \geq \sin \gamma$ ). This implies that

$$P[X > x] \leq e^{-\rho A_d} \leq e^{-\rho R x}, \quad (1)$$

which guarantees the promised asymptotic decay with  $c$ , for  $x = \frac{c}{\rho R}$ . In fact, the exponent of decay is approximately twice as large as that used in our proof: this follows because the values of  $x$ , and  $\gamma$ , we are considering are small, and  $A_d \sim 2xR$ , which yields  $P[X > x] \sim e^{-2\rho R x}$ .  $\square$

### 3.3 Remarks on Spatial Resolution Theorems

Theorems 1 and 2 show that the spatial resolution cannot be better than  $O(\frac{1}{\rho R})$ , and that this resolution can be achieved with a random (Poisson) sensor deployment. The dependence on sensor density seems to match common intuition: the more sensors we have, the better the spatial accuracy one should be able to achieve. On the other hand, the dependence on sensing radius may seem counterintuitive—because these are *binary proximity* sensors, they do not actually measure the distance to the target, and so having a large sensing radius may seem like a disadvantage. Indeed, as the sensing radius increases, we seem to get less information from an individual sensor: its 1 bit localizes the target to a larger area. Nevertheless, as our theorem shows, at the *system level*, the accuracy improves with larger sensing radius. This is a good example of the advantage of *networked* sensing, where the increase in an individual sensor’s uncertainty is counter-balanced by a *quadratic* increase in the number of patches into which the sensor field is partitioned by the sensing disks. When the sensing radius is small, the sensing disks are either disjoint or overlap only a little, and there are only  $O(n)$  patches. As the radius begins to grow, more disks pairwise intersect, and at sufficiently large radius, all pairs intersect, partitioning the sensor field into  $\Theta(n^2)$  patches, thereby reducing the size of each patch and improving the localization accuracy. In a finite sensor field, of course, this improvement stops when the radius becomes comparable to the length of the field.

Our theorems also help explain some of the empirical results of Kim et al. [12] for target tracking using binary proximity sensors. They found that for a fixed  $\rho R^2$  (which we can interpret as fixing the average number of sensors that can detect a target at a given position), better accuracy was achieved for the combination of “higher density and smaller

radius” than “lower density and larger radius,” leading them to propose that deployments with higher sensor density and smaller sensing radius are preferable. This empirical observation is a direct *consequence* of our theoretical results: for constant  $\rho R^2$ , reducing the sensing radius by 1/2 corresponds to a factor of 4 increase in the density, while reducing the density by 1/2 corresponds to  $\sqrt{2}$  increase in the radius. The former combination yields a higher value of  $\rho R$ , which implies better spatial resolution.

Finally, our resolution theorems easily generalize to any fixed dimension, and we can show that the achievable resolution in  $d$  dimensions is  $\Theta(1/(\rho R^{d-1}))$ .

### 3.4 Sampling and Velocity Estimation

The geometric information structure introduced in Section 2 shows that binary sensors can only localize the target to localization patches, and the resolution theorems of Section 3 show that these patches attain localization accuracy of  $\Delta = O(\frac{1}{\rho R})$ . Thus, as far as spatial accuracy is concerned, nothing further remains to be said. For any sequence of patch boundaries crossed by the target, there are infinitely many candidate trajectories crossing those patches in the same order, and *any one* of which is as good as another because they all lie within the achievable localization accuracy. Clearly, however, all these paths are not equally attractive as an estimate of trajectory. On grounds of “representational frugality,” perhaps one would prefer a path that uses a small number of segments as opposed to the one that uses a large number of segments. A different criterion may be to choose paths that track the second important quantity of interest in target tracking: its *velocity*. It turns out that these two topics (path representation and velocity estimation) are in fact closely related, and are the focus of this section.

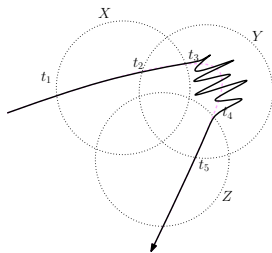


**Figure 4.** A trajectory exhibiting high frequency variations that cannot be captured by binary sensors.

Our starting point is an analogy between binary sensing and analog-to-digital conversion based on sampling and quantization, which immediately suggests that only a “low-pass” version of the trajectory can be reproduced. Consider, for instance, the trajectory shown in Fig. 4, which corresponds to the same sensor outputs as the trajectory of Fig. 1 but includes “high-frequency” variations around a slowly varying trend. Within the spatial resolution afforded by our sensor model, these two trajectories are indistinguishable. The high-frequency trajectory of Fig. 4, however, clearly has a higher velocity than the smooth trajectory of Figure 1. But, as we note below, the high-frequency component of its

velocity cannot be estimated based on binary sensor readings. This suggests that, among many spatially equivalent paths, piecewise linear approximations adequately represent the output of the sensor field in terms of both spatial resolution and velocity estimation. An analysis of velocity estimation errors using such piecewise linear representations leads to the intuitively pleasing conclusion that paths that use few segments (frugal representation) are also the paths that lead to good velocity estimation! These ideas lay the foundation for our algorithms (described in Section 4) that employ an Occam’s razor approach to the construction of estimated trajectories.

#### 3.4.1 Lowpass Trajectories

We begin with a simple but important interpretation of a binary sensor field as a device for spatial sampling. Let  $\mathbf{x}(t)$  denote the two-dimensional vector specifying the true location of the target at time  $t$ . Using the notation of Section 2, we can say that  $\mathbf{x}(t_j) \in A_j$ , where  $\{t_j\}$  are the times at which the target’s signature changes, and  $A_j$  is the arc defining the boundary between the patches  $F_j$  and  $F_{j+1}$ . For a moment, assume that a *genie* or an *oracle* actually tells us the precise locations  $\mathbf{x}(t_j)$ , for the set of time instants  $\{t_j\}$ . We can now infer the following about the velocity vector  $\vec{v}(t) = d\mathbf{x}/dt$ :

$$\int_{t_j}^{t_{j+1}} \vec{v}(t) dt = \mathbf{x}(t_{j+1}) - \mathbf{x}(t_j).$$

In other words, even with the genie’s aid, all that we can say about the target’s trajectory during the interval  $[t_j, t_{j+1})$  is that (i) the target is confined to the patch  $F_j$ , and (ii) the *average* vector velocity of the target in the patch is

$$\vec{v}_j = \frac{\mathbf{x}(t_{j+1}) - \mathbf{x}(t_j)}{t_{j+1} - t_j}$$

We denote the corresponding scalar average velocity by  $v_j = \|\vec{v}_j\|$ .

Note that we cannot infer anything about the deviation  $\vec{v}(t) - \vec{v}_j$  in the vector velocity from its average over the path, since this deviation integrates to zero in the time interval  $[t_j, t_{j+1})$ . This means that any high-frequency fluctuations in the path that are of small enough amplitude to stay within the patch  $F_j$  are entirely “invisible” to the binary sensor field.

Indeed, for a one-dimensional field of sensors, the sampling and quantization interpretation is immediate, without requiring invocation of a genie: the patches reduce to intervals and the arcs reduce to points. In this case, the binary sensor field is identical to a level-crossing analog-to-digital converter [19].

Therefore, at best we can hope to reconstruct a *lowpass representation* of the target’s trajectory, which we *define* as a piecewise linear approximation over spatial scale  $\Delta$ , with line segments connecting the sequence of points  $\mathbf{x}(t_1), \mathbf{x}(t_2), \dots$ . Other definitions that interpolate more smoothly across the arcs  $A_j$  are also possible, but the piecewise linear form has the virtue of being a minimal representation of the information obtained from the binary sensors and the genie (in particular, it preserves information in the average velocity sequence  $\{\vec{v}_j\}$ ).

The trajectory shape and the velocity estimates for the lowpass representation serve as a benchmark for comparing the output of any algorithm based on the sensor readings. Since this benchmark is defined with the genie's help (which eliminates the spatial uncertainty at each arc  $A_j$ ), it is not attainable in practice without some additional assumptions regarding the trajectory, as discussed in the next section.

### 3.4.2 Velocity Estimation Error

The set of all piecewise linear paths that visit the sequence of arcs  $A_j$  in the order given by the sensor signature sequence forms an equivalence class under the spatial resolution: all these paths are equivalent to the lowpass trajectory defined by the genie within the spatial resolution  $\Delta$ . Let us call this set REP, for spatial *Resolution Equivalence Paths* class. Even considering the lowpass representation, where all fluctuations of spatial scale smaller than  $\Delta$  are removed, two paths in REP can differ in length by a factor of 2: in a triangle of side length  $\Delta$ , there are two possible paths, one of length  $\Delta$  that follows one side, and one of length  $2\Delta$  following the other two sides. More generally, one path can be a straight line, and the other can zig-zag taking  $2\Delta$  long detours for each segment of length  $\Delta$  covered along the straight line.

In the absence of any other information, we simply have no way to decide which among the many candidate paths in the equivalence class REP offers the best approximation to the true path. The only way to decrease this uncertainty is to *assume* additional conditions that help shrink the spread of the path lengths in the equivalence class. In the following, we identify simple and natural *technical conditions* under which all the paths in the equivalence class have roughly the same length, and therefore any choice is guaranteed to give a good approximation. In particular, just as the accuracy of spatial resolution is controlled by size of the localization patches, the accuracy of the velocity estimation is controlled by the *variance in the path lengths of the equivalence class*.

We consider minimal representations of the trajectory in terms of piecewise linear approximations with line segments spanning several patches, and ask when velocity estimations computed using such a representation are accurate. That is, we seek conditions under which the entire class of equivalent paths provides a good approximation to the genie-aided average scalar velocity function, which is a piecewise constant sequence taking value  $v_j$  over the time interval  $[t_j, t_{j+1})$ .

We first relate the relative error in velocity estimation to the relative spread in path lengths in the equivalence class REP. Suppose that the estimated trajectory is of length  $L$  between arcs  $A_k$  and  $A_{k+m}$ . Assuming that the scalar velocity is constant over this path segment, it can be estimated as the length divided by the time to go between arcs  $A_k$  and  $A_{k+m}$ :  $v = L/(t_{k+m} - t_k)$ . Suppose the true trajectory between  $A_k$  and  $A_{k+m}$  has length  $L + \delta L$ . Then, our velocity estimate error is  $\delta v = \delta L/(t_{k+m} - t_k)$ . We therefore obtain that

$$\frac{\delta v}{v} = \frac{\delta L}{L} \quad (2)$$

That is, by considering the relative variation  $\frac{\delta v}{v}$  in velocity rather than the absolute variation  $\delta v$ , we are able to remove dependence on time scaling. The results we derive depend,

therefore, only on the spatial variations of the path shape and its velocity, and not on time scale.

The main consequence of Eq. (2) is that, if  $L$  is large enough and the permissible variation  $\delta L$  (constrained both by the sensor readings and the assumptions we make about the true trajectory) is small enough, then we can obtain accurate velocity estimates. For example, in order for a velocity estimate to be accurate to within 10%, we need to be able to guarantee that  $\delta L \leq 0.1L$ . If we assume that the scalar velocity is constant over large enough path sections, then we may be able to accurately estimate the velocity *as long as the variations in path lengths consistent with the sensor readings can be controlled*. Controlling the path length fluctuations is the same as bounding the path length spread in our equivalence class REP.

The following theorem characterizes the intrinsic ambiguity (caused by the spatial resolution  $\Delta$ ) in velocity estimation based on straight line approximations, arguing that the relative spread in path lengths is small if the line segment is long enough.

**THEOREM 3.** *Suppose a portion of the trajectory is approximated by a straight line segment of length  $L$  to within spatial resolution  $\Delta$ . Then, the maximum variation in the velocity estimate due to the choice of different candidate straight line approximations is at most*

$$\frac{\delta v}{v} \leq 2 \left( \frac{\Delta}{L} \right)^2.$$

*Furthermore, this also bounds the relative velocity error if the true trajectory is well approximated as a straight line over the segment under consideration.*

**PROOF.** By our spatial resolution theorem, the true trajectory is (approximately) a straight line that must lie within  $\Delta$  of the straight line approximation  $s$  we are considering. That is, it must lie in a rectangle of width  $2\Delta$  with  $s$  as its long axis. The maximum deviation in length from the approximation  $s$  is if the true trajectory is the diagonal of this rectangle, whose length is  $L + \delta L = 2\sqrt{(L/2)^2 + \Delta^2}$ , which yields  $\delta L \approx 2\frac{\Delta^2}{L}$  for  $\Delta \ll L$ . Clearly, this bound also applies for deviation of the true trajectory from the straight line approximation being considered, as long as the true trajectory is well approximated as a straight line over the current segment. We now apply Eq. (2) to obtain the desired result.  $\square$

Theorem 3 implies that, if we want to control the relative velocity error to less than  $\epsilon$  using a piecewise linear approximation, then the length of each line segment must be at least

$$L \geq L_0 = \frac{\sqrt{2}\Delta}{\sqrt{\epsilon}}. \quad (3)$$

As an example, to achieve error at most 10%, segments of length  $5\Delta$  suffice; error of 5% requires segments of length  $\approx 6.32\Delta$ . Put another way, if on average each linear approximation segment spans  $\alpha$  localization arcs, then the average relative velocity error is  $dv/v \leq 2/\alpha^2$ . Our simulation results show that even for fairly complex (synthetic) trajectories, a piecewise linear approximation works well, with  $\alpha$  at least 10 on average.

Note that, for trajectories that “wiggle” while staying within  $\Delta$  of a (long enough) straight line, Theorem 3 can be interpreted as guaranteeing accuracy in estimation of the *projection* of the velocity along the straight line. On the other hand, if a trajectory *curves* sharply, piecewise linear approximations to within  $\Delta$  of the trajectory must necessarily use shorter line segments, making the velocity estimation error worse. But this is unavoidable because over short spans, the relative difference between two linear segments is larger, as implied by Theorem 3: in the extreme case, where  $L \approx \Delta$ , we are back to the factor of two error discussed at the beginning of Section 3.4.2.

## 4 Tracking Algorithms

The theoretical considerations of the previous section motivate an Occam’s razor approach to tracking. Among all the candidate paths meeting the spatial resolution bound, a piecewise linear approximation that uses a minimal number of segments has the advantage of compact representation as well as accurate velocity estimation. Using the notation of Section 2, we know that the target is constrained to lie in region  $F_j$  during the time interval  $[t_j, t_{j+1}]$ , where  $\{t_j\}$  are the time instants at which there are changes in the bit vector of sensor outputs. We formally define a localization region  $F_j$ , corresponding to an interval  $[t_j, t_{j+1}]$ , as follows, dropping the subscript  $j$  for convenience. Let  $I$  be the subset of sensors whose binary output is 1 during the relevant interval, and let  $Z$  be the remaining sensors whose binary output is 0 during this interval. Then the region  $F$  of the plane to which the target can be localized during this interval is given as:

$$F = \bigcap_{i \in I} D_i - \bigcup_{i \in Z} D_i,$$

where  $D_i$  is the sensing disk of radius  $R$  centered at sensor  $i$ . Note that it is not necessary to consider the entire set  $Z$  in order to determine  $F$ : it suffices to consider only those sensors whose disks can intersect with any disk in  $I$ . Thus, in our implementation, it is necessary only to maintain, for each sensor  $s$ , a *neighbor list* of all other sensors whose sensing disks intersect with the disk of  $s$ .

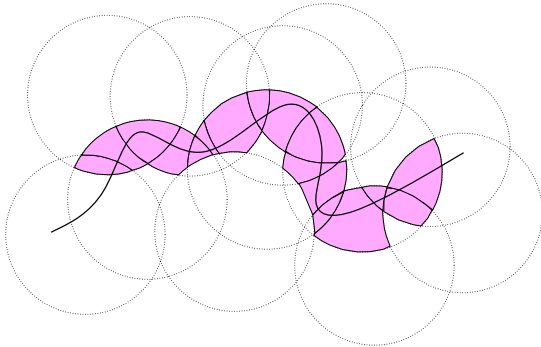


**Figure 5.** The shaded band shows the regions  $\{F_i\}$  to which the trajectory is localized by the sensor outputs.

Fig. 5 shows an example trajectory and the band consisting of the regions. Any trajectory that traverses these regions

in the order specified by the sensing outputs is consistent with the target’s true trajectory, within the accuracy bounds of the model. Among all these possible trajectories, the Occam’s razor approach prefers the one that is the simplest. For instance, if all the regions could be traversed by a single line, then a linear trajectory has the simplest descriptive complexity, within the theoretical accuracy of tracking. Generalizing this, a *piecewise linear* trajectory with the fewest number of linear segments that traverses all the sensed regions in order is the trajectory of minimal complexity. In the following section, we describe a geometric algorithm, OCCAMTRACK, for computing such a trajectory. Our computational model assumes that a tracker node collects the output from the sensor nodes, and runs the algorithm to compute the trajectory. The algorithm, however, can also be implemented in a distributed fashion by exchanging data among the neighboring nodes.

### 4.1 The OCCAMTRACK Algorithm

Algorithm 1 below describes the OCCAMTRACK at a pseudo-code level.  $S$  is the set of all the sensors, and the algorithm operates in discrete time steps  $T$ , which are simply the instants at which one of the sensor’s binary state changes. At each of these discrete time steps  $t$ , the algorithm determines the sets  $I$  and  $Z$ , and computes the region  $F$  localizing the target. The *time-ordered* sequence of these regions  $F$  is the *spatial band*  $B$  that contains the target’s trajectory. The function MINSEGPATH then computes a minimum piecewise linear path traversing the band.

---

#### Algorithm 1 OCCAMTRACK( $S$ )

---

- 1:  $T \leftarrow \{s.start, s.end : \forall s \in S\}$ ;
  - 2:  $sort(T)$ ;
  - 3: **for all**  $t \in T$  **do**
  - 4:  $I \leftarrow \{s : t \in [s.start, s.end]\}$ ;
  - 5:  $Z \leftarrow \{s : s \in I.nbrlist \wedge t \notin [s.start, s.end]\}$ ;
  - 6:  $F \leftarrow \bigcap_{i \in I} D_i - \bigcup_{i \in Z} D_i$ ;
  - 7:  $B \leftarrow B \cup F$ ;
  - 8: **end for**
  - 9:  $L \leftarrow MINSEGPATH(B)$ ;
- 

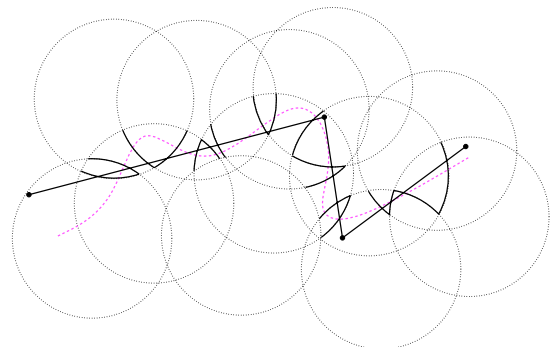


**Figure 6.** The path computed by OCCAMTRACK has 3 line segments. The sequence of arcs delineating the regions of band  $B$  are shown in thick lines.



In the pseudo-code for MINSEGPATH, the function FINDARCS determines the ordered sequence of localization arcs corresponding to the localization band  $B$ .<sup>3</sup> The function FINDLINE either determines that a subsequence of arcs  $q_i, q_{i+1}, \dots, q_j$  cannot be “stabbed” (in the given order) by a single line, or finds such a stabbing line. The algorithm MINSEGPATH uses this function in a greedy fashion to find the longest prefix of arcs that can be approximated by a single line segment, removes those arcs, and then iterates on the remaining sequence. There are only a finite number of combinatorially distinct candidate lines one needs to test to decide if a sequence of arcs can be stabbed by a line. In particular, it suffices to test the lines formed by pairs of endpoints of arcs, or lines that are tangent to some arc.<sup>4</sup> Figure 6 shows the minimal description path for the example of Figure 5.

---

**Algorithm 2** MINSEGPATH( $B$ )

---

```

1:  $A \leftarrow \text{FINDARCS}(B)$ ;
2:  $i \leftarrow 1$ ;
3: for all  $j \in \{1, 2, \dots, m\}$  do
4:   if  $\neg \text{FINDLINE}(A_i, A_{i+1}, \dots, A_j)$  then
5:      $L \leftarrow \text{LUFINDLINE}(A_i, A_{i+1}, \dots, A_{j-1})$ ;
6:      $i \leftarrow j$ ;
7:   end if
8: end for

```

---

## 4.2 Analysis of OCCAMTRACK

By construction, the piecewise linear path computed by OCCAMTRACK intersects the regions of the band  $B$  in the same order as given by the binary sensors outputs—this follows because MINSEGPATH constrains the path to visit the boundary arcs of consecutive regions in order. This, however, does not mean that the true trajectory and the piecewise linear path visit the *same sequence* of regions. The linear shortcuts found by OCCAMTRACK can visit additional regions. This can happen if the linear segment crosses over a *non-convex* vertex of one of the regions. The important point to note, however, is that the maximum distance between the true trajectory and the computed path at any instant (the  $L_\infty$  error) is still bounded by  $\Delta = O(1/\rho R)$ , because the path computed by OCCAMTRACK does lie entirely within the union of the *convex hulls* of the  $F$  regions in the band  $B$ . Since the diameter of the convex hull of any  $F$  region is bounded by  $\Delta$ , the error guarantee follows. The following

<sup>3</sup>While a localization arc can have multiple pieces in a pathological case, the union of all its sub-arcs is still within the resolution bound (cf. Theorem 2). Thus, for the purpose of minimal path representation, we can safely “interpolate” all the disconnected pieces of the arc and still remain within the tolerable error. However, to keep our implementation simple, we chose to ignore such pathological contingencies, and opted to simply ignore an arc if it were found to be disconnected.

<sup>4</sup>In computational geometry, several theoretically more efficient methods (e.g. [8]) are known for these stabbing problems, but they are complicated to implement and involve significant overhead in data structures. We chose to implement our algorithm because it is simple, compact, works fast in practice.

theorem shows that the worst-case path approximation computed by MINSEGPATH uses at most twice the number of optimal segments. (In practice, it is very close to optimal.) Due to lack of space, we omit the proof of this theorem.

**THEOREM 4.** *The algorithm OCCAMTRACK computes a piecewise linear path that visits the localization arcs in order and uses at most twice the optimal number of segments in the worst-case. If there are  $m$  arcs in the sequence, then the worst-case time complexity of OCCAMTRACK is  $O(m^3)$ .*

## 4.3 Robust tracking with non-ideal sensors

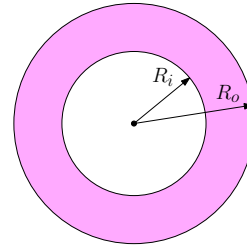


**Figure 7.** The non-ideal sensing model

The OCCAMTRACK algorithm assumes ideal binary sensing. In practice, sensing is imperfect and noisy: a sensor could detect an object outside its nominal range, or it may fail to detect an object inside its range. We illustrate our approach to such non-idealities using a sensing model in which the target is always detected within an inner disk of radius  $R_i$ , called the *detection region*, and is detected with some nonzero probability in an annulus between the inner disk and an outer disk of radius  $R_o$ , called *uncertain region*. Targets outside the outer disk are never detected. Figure 7 gives an illustration of this model. Despite its simplicity, such a model is of fairly broad applicability, since it arises naturally if sensors integrate noisy samples over a reasonable time scale to make binary decisions regarding target presence or absence.

The main implication of the model in Figure 7 for the OCCAMTRACK algorithm is that we can no longer identify circular arcs corresponding to an object entering and leaving a sensor’s detection range. While we can employ OCCAMTRACK algorithm directly by approximating the sensing region as a disk of some radius  $R$ , where  $R_i \leq R \leq R_o$ , simulations show that the performance can be poor. We therefore consider an alternative approach, in which we employ a particle filtering algorithm to handle non-idealities. While this produces a good approximation of the true trajectory, it is not amenable to an economical description. We therefore employ a geometric post-processing algorithm to obtain a minimal representation for the output of the particle filtering algorithm. While particle filtering is a well established technique, the main novelty of the algorithm presented here is the way in which it exploits the constraints of the sensing model for a simple and efficient implementation.

In order to illustrate robustness to non-ideal sensing, we take a worst-case approach to the information provided by the non-ideal sensing model in Figure 7, assuming the maximal uncertainty consistent with the sensor readings. If a

sensor output is 1, then we assume that the target is somewhere inside the large disk of radius  $R_o$  centered at the sensor. If a sensor output is 0, then we assume that the target is somewhere outside the small disk of radius  $R_i$  centered at the sensor. A localization patch  $F$  at any time instant is given by intersecting all such areas, just as before.

### 4.3.1 Particle Filtering Algorithm

We now sketch the particle filtering algorithm; a more detailed description and software implementation is available from the authors upon request. At any time  $n$ , we have  $K$  particles (or candidate trajectories), with the current location for the  $k$ th particle denoted by  $x_k[n]$ . At the next time instant  $n + 1$ , suppose that the localization patch is  $F$ . Choose  $m$  candidates for  $x_k[n + 1]$  uniformly at random from  $F$ . We now have  $mK$  candidate trajectories. Pick the  $K$  particles with the best cost functions to get the set  $\{x_k[n + 1], k = 1, \dots, K\}$ , where the cost function is to specified shortly. Repeat until the end of the time interval of interest. The final output is simply the particle (trajectory) with the best cost function. Thus, Monte Carlo simulation is an intrinsic part of this algorithm, since random sampling is employed to generate candidates for evaluation. The sampling time interval is chosen to be short compared to a localization patch, so as to generate a sufficiently rich set of candidates.

It remains to specify the cost function. We chose an additive cost function that penalizes changes in the vector velocity, in keeping with our restriction to lowpass trajectories. Once a candidate  $x_k[n + 1]$  is chosen from the current localization patch, the increment in position  $x_k[n + 1] - x_k[n]$  is an instantaneous estimate of the velocity vector at time  $n$ . The corresponding increment in the cost function is the norm squared of the difference between the velocity vector estimates at time  $n$  and  $n - 1$ . This is given by

$$c_k[n] = \|(x_k[n + 1] - x_k[n]) - (x_k[n] - x_k[n - 1])\|^2 \\ = \|x_k[n + 1] + x_k[n - 1] - 2x_k[n]\|^2$$

The net cost function for a candidate trajectory up to time  $n$  is simply the sum of these incremental costs:  $\sum_{m=1}^n c_k[m]$ .

### 4.3.2 Geometric Postprocessing

The particle filtering algorithm described above gives a robust estimate of the trajectory consistent with the sensor observations, but it provides no guarantees of a “clean” or minimal description. This suggests the possibility of applying the geometric approach of Section 4.1 to the particle filter estimate to generate a more economical description. We omit details due to lack of space, but provide a brief pseudo-code description of an algorithm FITLINE to generate a piecewise linear approximation with a small number of line segments. In the pseudo-code,  $p$  is the ordered list of samples generated by the particle filtering algorithm,  $L$  is the output piecewise linear approximation, and function LINESEGMENT( $Q$ ) returns a line segment that is within distance  $\Delta$  of the sequence of points  $Q$ .

---

### Algorithm 3 FITLINE( $p$ )

---

```

1:  $Q \leftarrow \phi$ ;
2: for all  $i \in 1, 2, \dots, |p|$  do
3:   if ERROR( $Q \cup p_i$ )  $> \Delta$  then
4:      $L \leftarrow L \cup \text{LINESEGMENT}(Q)$ ;
5:      $Q \leftarrow \phi$ ;
6:   end if
7:    $Q \leftarrow Q \cup p_i$ ;
8: end for

```

---

## 5 Simulation Results

We carried out extensive simulation tests to evaluate the performance of all our algorithms, under both ideal and non-ideal sensing models. The code for OCCAMTRACK was written in C and C++, the code for PARTICLE-FILTER was written in Matlab, and the experiments were performed on an AMD Athlon 1.8 GHz PC with 350 MB RAM. We first discuss our results for the ideal sensing model.

### 5.1 OCCAMTRACK with ideal sensing

Our general experimental setup simulated a  $1000 \times 1000$  unit field, containing 900 sensors in a regular  $30 \times 30$  grid. The sensing range for each sensor was set to 100 units. When evaluating the scaling affects of the sensor parameters, we kept the field size and one parameter fixed, while the other parameter (radius or density) was varied.

We used *geometric random walks* to generate a variety of trajectories. Each walk consists of 10 to 50 steps, where each step chooses a random direction and walks in that direction for some length, before making the next turn. Each trajectory has the same total length, and we generated 50 such trajectories randomly.

#### 5.1.1 Quality of trajectory approximation

On all 50 random walk trajectories, OCCAMTRACK delivers excellent performance. Figure 8(b) is a typical example, where the true trajectory is virtually indistinguishable from the approximation computed by OCCAMTRACK.

We also ran the weighted-centroid algorithm of Kim et al. [12] on these trajectories. In our comparison, we used the *adaptive path-based* version of their algorithm, which is claimed to be well-suited for complex and non-linear trajectories. For ease of reference, however, we still refer to this algorithm as the *weighted-centroid* scheme. We ran this algorithm with inner and outer radii both equal to the ideal radius 100.

Figure 8(a) shows the output of the weighted-centroid method, and is typical of its performance on all our random walk trajectories. The weighted-centroid algorithm is sample based, and it used 1000 vertices to approximate each of the trajectories. By contrast, the OCCAMTRACK used between 20 and 70 vertices. Despite this frugal representation, the maximum localization error for OCCAMTRACK was *always* smaller than the weighted-centroid, on average by 30%, and in some cases by a *factor of five*. Due to its highly efficient structure, OCCAMTRACK is also 300 times faster than weighted-centroid. In all cases, our algorithm

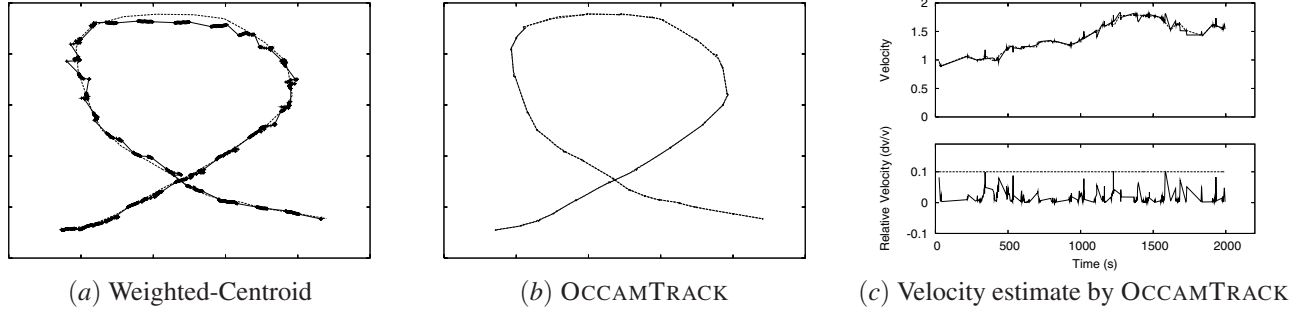


**Figure 8. Quality of trajectories produced by the weighted-centroid algorithm of [12] and OCCAMTRACK. Figure (c) shows the results of velocity estimation by OCCAMTRACK.**

took less than 10 milliseconds, while weighted-centroid took between 2 and 20 seconds.

### 5.1.2 Velocity estimation performance

In our random walk trajectories, we also varied the scalar velocity randomly at each turn, and then used OCCAMTRACK to estimate the scalar velocity along the trajectory. For each linear segment in the piecewise linear path computed by OCCAMTRACK, we used the first and the last localization arc to determine the time spent on that segment; recall that sensor outputs tell us the exact times for each arc. We estimate the scalar velocity for this segment by dividing the length of the segment by this time. With a goal of estimating the velocity within  $\epsilon = 0.1$ , namely, 10%, we estimated the average velocity only over path segments of length at least  $L = \sqrt{2}\Delta/\sqrt{\epsilon}$ , as given by Eq. 3.

In Figure 8(c), we show the results of estimating the velocity for the sample trajectory of (b). The top figure shows the overlay of both the true and the estimated velocities along the trajectory, and one can see that the two agree very well. In the bottom figure, we plot the relative error in the velocity to highlight deviation. The figure shows that the maximum deviation is always less than 10%, as predicted by theory.

The results were very similar for all 50 trajectories. In particular, on average a segment of OCCAMTRACK’s trajectory spanned about 15 patches, meaning that an average line segment in the approximation has length  $L = 15\Delta$ , meaning that the velocity estimates are good, as explained by Theorem 3.

In the following two experiments, we evaluated the localization accuracy of OCCAMTRACK with varying  $\rho$  and  $R$  over many random trajectories, to see how it compares to the theoretical predictions of our theorems.

### 5.1.3 Spatial resolution as a function of density

In this experiment, we measured the maximum error in localizing the target’s trajectory for a varying values of the sensor density. We kept the size of the field and the sensing radius  $R$  fixed, and then varied the number of sensors in the field from  $n = 100$  to  $n = 6400$ . (Since the area of the field is  $10^6$ , this corresponds to variation in density from  $10^{-4}$  to  $6.4 \times 10^{-3}$ .) We tried both the regular grid arrangement of the sensors, as well as the random placement.

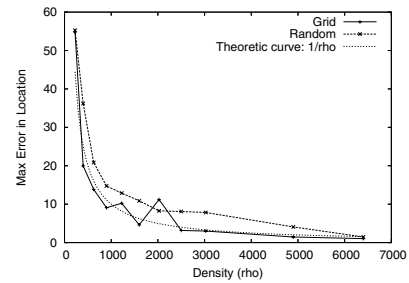


**Figure 9. Spatial resolution vs. sensor density.**

By the spatial resolution theorem, the localization error should decrease inversely with the density. Figure 9 shows that the measured error follows closely the theoretical curve of  $1/\rho$ , both for the grid as well as the random placement. In each case, the reported error is the maximum error for the trajectory, averaged over 50 random walk trajectories. (The average error for each trajectory is much smaller.)

### 5.1.4 Spatial resolution as a function of sensing range

In this experiment, we kept the density constant at 900 nodes in the field, and varied the sensing radius from 50 to 400 units. Figure 10 shows the maximum error, averaged over 50 random walk trajectories, for various values of the sensing range. By the spatial resolution theorem, the localization error should decrease inversely with the sensing range, and again the measured values closely follow the theoretical curve of  $1/R$ .

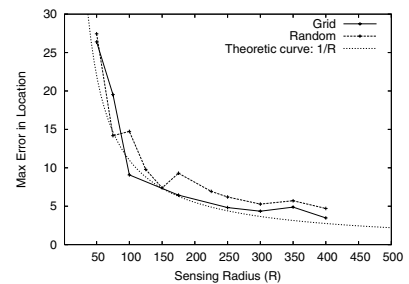


**Figure 10. Spatial resolution vs. sensing radius.**

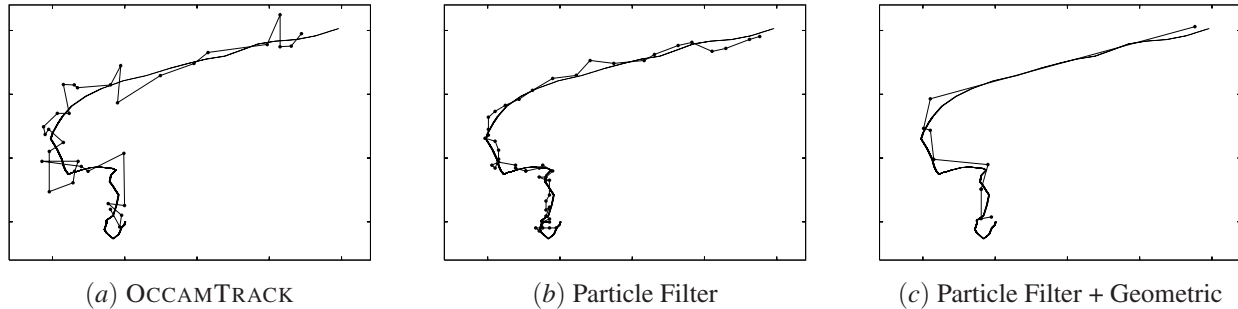


Figure 11. Trajectories computed by the three algorithms under the non-ideal sensing model.

## 5.2 Tracking with Non-Ideal Sensing

We now describe the results of our experiments with non-ideal sensors. Our model of non-ideal sensors is the one shown in Figure 7, where in the region between distance  $R_i$  and  $R_o$ , the target is detected with probability  $\frac{1}{2}$ . An imperfect detection is problematic for the ideal geometric algorithm OCCAMTRACK because it relies on contiguous time intervals during which the target is inside the range. We used a simple hysteresis process to mitigate the affect of erratic detection: to signal the beginning of a detection interval, we require the sensor to output a 1 bit for 3 consecutive time samples; similarly, to signal the end of a detection interval, we require the sensor to output a 0 bit for 3 consecutive time samples.

We generated a variety of geometric trajectories, simulated the sensor outputs using our non-ideal sensing model, and ran OCCAMTRACK, PARTICLE-FILTER, and PARTICLE-FILTER with geometric post-processing, which we call PARTICLE FILTER + GEOMETRIC. A sample trajectory, along with the outputs of the three algorithms, is shown in Figure 11.

As expected, the ideal algorithm OCCAMTRACK performs poorly when the data is imperfect: such data lead to gaps in the sequence of localization patches and infeasible localization arcs. In our implementation, we simply *ignored* these geometric inconsistencies, and just computed the piecewise linear paths using the rest of the arcs. Of course, in the worst-case, poor data can completely break OCCAMTRACK, but we found that the algorithm recovers rather well from these bad situations and produces acceptable trajectories, although not nearly as good as in the ideal case. In fact, compared to PARTICLE-FILTER, the output of OCCAMTRACK looks significantly worse: it has significantly more pronounced turns and twists. PARTICLE-FILTER seems much better at dealing with noisy data, but its drawback is that, like any sample-based scheme, it produces trajectories with many vertices. This is where our combination of PARTICLE-FILTER with geometric post-processing achieves the best of both worlds: it combines the robustness of PARTICLE-FILTER with the economic paths of the ideal OCCAMTRACK.

In particular, in the example of Figure 11, the output of PARTICLE-FILTER + Geometric uses 10 segments and has maximum error of 1.73, compared to 51 segments required



Figure 12. The setup for our acoustic motes experiment.

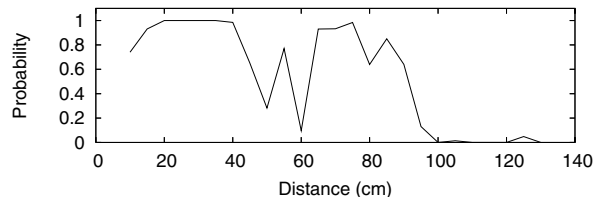


Figure 13. Probability of target detection with distance for an acoustic sensor.

for the PARTICLE-FILTER for the error of 1.19. We simulated this experiment over several trajectories, using the non-ideal sensing, and observed the same trend. On a typical input, the maximum localization error using PARTICLE-FILTER + Geometric was comparable to the basic particle filter algorithm, but in the worst-case it was almost 50% higher. On the other hand, the path description computed by PARTICLE-FILTER + Geometric was at least a *factor of 5* smaller.

## 6 Mote Experiments

Finally, we set up a small lab-scale experiment using acoustic sensors to evaluate the performance of our algorithms. The setup consisted of 16 MICA2 motes arranged in a  $4 \times 4$  grid with 30 centimeter separation, as shown in Figure 6. The motes were equipped with a MTS310 sensor board, which has an acoustic sensor and a tone detector circuit. (The tone detector can detect acoustic signals in a specific frequency range.) We adjusted the gain of the sound sensor so that the detection range for each sensor is

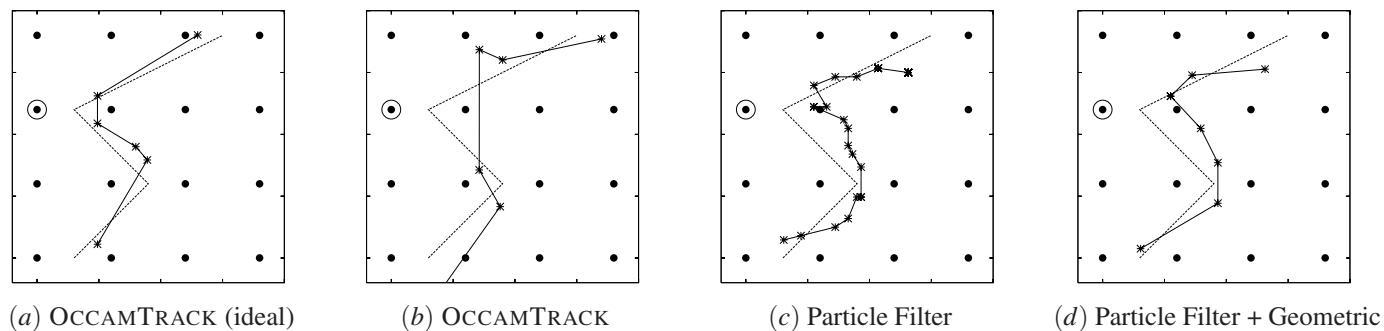


Figure 14. The output trajectories for the experiment using acoustic sensors.

about 45 cm. The target is also a MICA2 equipped with MIB310, which generated the acoustic signal using its on-board *beeper*. The target is then moved through the network in a path (shown as the dotted trajectory in Fig. 14).

We first performed some experiments with a stationary target to determine the detection characteristics of the motes’ tone-detector. The readings from the motes turned out to be highly non-ideal. Not only did the motes make frequent detection errors, but the probability of detecting a target was not a monotonic function of the distance from the sensor, as shown in Fig. 13. While this detection behavior is difficult to model, it also means that this experiment is a good test for the robustness of our tracking algorithms.

The results of our experiment are shown in Fig. 14. The detection readings we collection from these experiments showed a lot of non-ideal behavior. The most extreme being that one of the sensors, shown as double circle in the figure, failed to detect the target *entirely*, even though the target comes very close to it.

On the whole, however, even in presence of such extreme failures, the results are very encouraging. All three algorithms were able to give a reasonable estimate of the target track. Figure 14(a) shows the reference output for OCCAMTRACK, assuming ideal sensing—that is, assuming the faulty sensor had also detected correctly, this is the trajectory OCCAMTRACK would produce. The other three figures show the outputs using the actual measurements from the acoustic sensors. (The actual path of the target is shown as a dotted line, while the estimated trajectories are shown in bold lines.) As expected, the trajectory quality of OCCAMTRACK suffers the most because of the failed sensor. The PARTICLE-FILTER does better, and again the combined algorithm preserves the robustness of PARTICLE-FILTER and approaches the minimal path description of OCCAMTRACK.

## 7 Closing Remarks

We have identified the fundamental limits of tracking performance possible with binary proximity sensors, and have provided algorithms that approach these limits. The results show that the binary proximity model, despite its minimalism, does indeed provide enough information to achieve respectable tracking accuracy, assuming that the product of the

sensing radius and sensor density is large enough. Thus, this model can serve as a building block for broadly applicable and reusable tracking architectures.

The promising results obtained here and in [12], as well as the success of the large-scale deployment in [1], motivate a more intense investigation of tracking architectures based on the binary proximity model. In order to focus on fundamentals, we have considered a single path in our simulations and experiments. An in-depth understanding, and accompanying algorithms, for multiple targets is therefore an important topic for future investigation. We would also like to develop minimal modifications of the basic tracking architecture to incorporate additional information (e.g., velocity, distance) if available. The particle filtering framework appears to be a promising means for achieving this. In addition to extensions and implementation optimization of this framework, an interesting question is whether it is possible to embed Occam’s razor criteria in the particle filtering algorithm, rather than using geometric post-processing to obtain economical path descriptions.

## Acknowledgment

We are grateful to the authors of [12] for giving us access to their target tracking code.

## 8 References

- [1] A. Arora, P. Dutta, S. Bapat, V. Kulathumani, H. Zhang, V. Naik, V. Mittal, H. Cao, M. Demirbas, M. Gouda, Y. Choi, T. Herman, S. Kulkarni, U. Arumugam, M. Nesterenko, A. Vora, and M. Miyashita. A line in the sand: a wireless sensor network for target detection, classification, and tracking. *Comput. Networks*, 46(5):605–634, 2004.
- [2] J. Aslam, Z. Butler, F. Constantin, V. Crespi, G. Cybenko, and D. Rus. Tracking a moving object with a binary sensor network. In *ACM SenSys*, 2003.
- [3] R. Chellappa, Gang Qian, and Qinfen Zheng. Vehicle detection and tracking using acoustic and video sensors. In *Proc. of IEEE Conf. on Acoustics, Speech, and Signal Processing*, volume 3, pages iii–793–6, 2004.

- [4] M. Coates. Distributed particle filters for sensor networks. In *Proc. IPSN*, pages 99–107, 2004.
- [5] A. Doucet, S. Godsill, and C. Andrieu. On sequential monte carlo sampling methods for bayesian filtering. *Statistics and Computing*, 10(3):197–208, 2000.
- [6] J. Elson, L. Girod, and D. Estrin. Fine-grained network time synchronization using reference broadcasts. *SIGOPS Oper. Syst. Rev.*, 36:147–163, 2002.
- [7] D. Fox, S. Thrun, W. Burgard, and F. Dellaert. Particle filters for mobile robot localization. In Arnaud Doucet, Nando de Freitas, and Neil Gordon, editors, *Sequential Monte Carlo Methods in Practice*, New York, 2001. Springer.
- [8] L. Guibas, J. Hershberger, J. Mitchell, and J. Snoeyink. Approximating polygons and subdivisions with minimum link paths. In *ISAAC*, 1991.
- [9] S.A. Ketcham, M.L. Moran, J. Lacombe, R.J. Greenfield, and T.S. Anderson. Seismic source model for moving vehicles. *IEEE Trans. on Geoscience and Remote Sensing*, 43(2):248–256, 2005.
- [10] Z. Khan, T. Balch, and F. Dellaert. Efficient particle filter-based tracking of multiple interacting targets using an MRF-based motion model. In *Proc. IEEE/RSJ International Conference on Intelligent Robots and Systems*, volume 1, pages 254–259, 2003.
- [11] Z. Khan, T. Balch, and F. Dellaert. MCMC-based particle filtering for tracking a variable number of interacting targets. *IEEE Transactions on Pattern Analysis and Machine Intelligence*, 27(11):1805–1819, 2005.
- [12] W. Kim, K. Mechitov, J.-Y. Choi, and S. Ham. On target tracking with binary proximity sensors. In *Proc. IPSN*, 2005.
- [13] J. Liu, P. Cheung, L. Guibas, and Feng Zhao. Apply geometric duality to energy efficient non-local phenomenon awareness using sensor networks. *IEEE Wireless Communication Magazine*, 11:62–68, 2004.
- [14] D. McErlean and S. Narayanan. Distributed detection and tracking in sensor networks. In *Proc. of 36th Asilomar Conference on Signals, Systems and Computers*, volume 2, pages 1174–1178, 2002.
- [15] C. Meesookho, S. Narayanan, and C. S. Raghavendra. Collaborative classification applications in sensor networks. In *Proc. of Workshop on Sensor Array and Multichannel Signal Processing*, pages 370–374, 2002.
- [16] B. S. Y. Rao, H. F. Durrant-Whyte, and J. A. Sheen. A fully decentralized multi-sensor system for tracking and surveillance. *Int. J. Rob. Res.*, 12(1):20–44, 1993.
- [17] A. M. Sabatini, V. Genovese, E. Guglielmelli, A. Mantuano, G. Ratti, and P. Dario. A low-cost, composite sensor array combining ultrasonic and infrared proximity sensors. In *Proc. Int. Conference on Intelligent Robots and Systems*, volume 3, pages 120–126, 1995.
- [18] A. Savvides, C.-C. Han, and M. B. Strivastava. Dynamic fine-grained localization in ad-hoc networks of sensors. In *Proc. Mobicom*, pages 166–179, 2001.
- [19] N. Sayiner, H.V. Sorensen, and T.R. Viswanathan. A level-crossing sampling scheme for a/d conversion. *IEEE Transactions on Circuits and Systems*, 43(4):335–339, 1996.